

Embracing Self-Powered Wireless Wearables for Smart Healthcare

Lonzhi Yuan[†], Can Xiong[†], Si Chen[‡], and Wei Gong^{†*}

[†]University of Science and Technology of China; [‡]Simon Fraser University
lonzhi@mail.ustc.edu.cn, canxiong@ustc.edu.cn, sca228@sfsu.ca, weigong@ustc.edu.cn

Abstract—We present Apollo, a self-powered wireless biochemical system that is wearable and can continuously monitor personal health states. It has three key enablers. First, we design an ultra-low-power Bluetooth backscatter module, which can effectively take BLE signals as excitations and transmit sensor data at high data rates to smartphones. Further, at the core of self-power management is a novel multi-source harvester that can transform RF, light, and thermal energies into electrical energy. Moreover, we introduce a biochemical sensor array that can accurately measure sweat metabolites and electrolytes.

We prototype Apollo on a compactly integrated flexible PCB using all commercial off-the-shelf components. Through extensive experiments and field studies, we show that it is able to measure the glucose level in sweat within 5% error rate while consuming 5.8 mW for sensing and 720 pJ/bit for wireless transmissions. This translates to over 1700x lower power than standard electrochemical workstations, and 26x lower power than existing commercial BLE chipsets. We believe Apollo marks an important step towards the dream of ubiquitous healthcare for everyone as it provides a highly convenient, self-managed, and fully integrated way for health monitoring.

Index Terms—biosensors, sweat, backscatter, energy harvesting

I. INTRODUCTION

Sweat tells us a lot about human health. Sweat glucose can serve as an attractive candidate for diabetes management; sweat lactate is reported to be a sensitive marker for pressure ischaemia; abnormal concentration of sodium and potassium in sweat could be related to the hyponatremia/hypernatremia and hypokalemia/hyperkalemia; sweat chloride level is currently considered the gold standard for cystic fibrosis diagnosis. So it's of great importance to continuously monitor human sweat.

A useable sweat sensing system should satisfy three requirements besides its effectiveness in analyzing human perspiration: wearable, long-range, and self-powered.

1) Wearable Miniaturized and portable are not enough. A rigid system needs the user to pay attention to maintain the working condition, and being wearable means reliable and additional maintenance can be avoided.

2) Self-powered Frequently charging and maintaining batteries is disturbing and costly. So providing power by itself is very important. The sweat sensing system should be able to gather energy from the environment or human body.

3) Long-range The long data transmission range broadens the usage of the sensing system. So that we don't need to

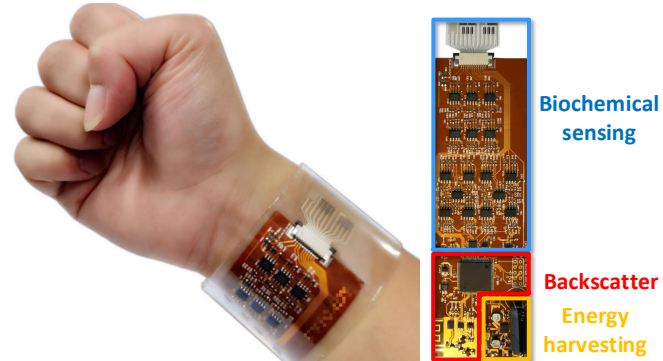


Fig. 1. Wearable sweat analyzing system.

keep a smartphone or tablet very close to the sensing system, and work or exercise normally.

There are many works trying to provide an easier way to monitor biomarkers [1] [2] [3] [4]. Those works make great progress towards realizing miniaturization and usability of biosensor systems. But none of them satisfies all three requirements. In [1] a battery is used for power supply and a USB interface is used for communication; in [2] [3] the system is powered by a battery; the work in [4] gets rid of battery by integrating NFC technology, but it's still limited in working range.

Backscatter is attractive for its low power and low cost, an example is RFID [5] [6] [7] [8] [9] [10]. It needs a carrier provider and a receiver to realize communication. Many works have made it possible to use commercial devices as the carrier provider and receiver [11] [12] [13] [14] [15] [16] [17] [18].

So we build our biosensor system Apollo to cover those requirements. Our sweat sensing system is built in a wristband-shaped flexible PCB. All components including electronic components and the customized sensor array are mounted on the top surface and the biosensor system is wearable. Further, Apollo is able to harvest energy from the RF signal, light, and heat source. Such multiple-source harvester design improves the harvesting performance and broadens the application scenarios. When one or two energy sources are absent the system can still gather energy and function well. To realize long-range communication with the least amount of power we integrate Bluetooth backscatter in the system. The backscatter module is enabled to identify the BLE signals from other interferences

*Corresponding author: Wei Gong.

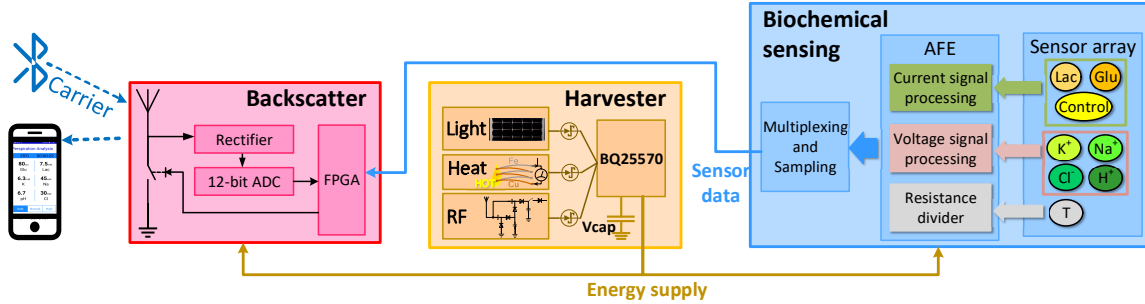


Fig. 2. System overview. Apollo biosensor system is functionally composed of three modules: backscatter communication module, energy harvesting and management module.

such as WiFi and ZigBee sharing the 2.4GHz ISM band. The sensor data is transmitted to the smartphone with the help of the identified BLE packets. The sensor array is sensitive to concentrations of glucose, lactate, K^+ , Na^+ , H^+ , and Cl^- , and the concentrations can be estimated by measuring the generated current or voltage.

In conclusion, our contribution is combining biochemical technique, backscatter communication, and energy harvesting to demonstrate the feasibility of noninvasive wearable biochemical sensing.

II. SYSTEM OVERVIEW

Fig. 2 shows the overview of our self-powered human sweat monitoring system. It's structured in a flexible PCB and functions as a wristband. There are three modules: the biochemical sensing module, the backscatter communication module, and the energy harvesting module. As can be seen that the biochemical sensing module including the sensor array and the signal processing paths covers more than two-thirds of the PCB area. The backscatter communication module and the energy harvesting module cover about three quarters and one-quarter of the rest area, respectively. The energy converters including the solar panel, the thermoelectric generator (TEG) for heat energy, and the rectifier for RF energy are not shown in real pictures. We will introduce those modules in detail.

The backscatter module detects ongoing BLE packets and manipulates the toggling of RF-switch to piggyback sensor readings onto those packets. The Frontend in Backscatter module contains an RF-switch and a BLE baseband extracting and sampling circuit. The energy harvesting module is responsible for gathering energy from ambient light energy, ambient RF energy, and ambient heat energy using energy convertors. A large capacitor instead of a battery is used as the energy storage component in the system. The biochemical sensing module includes the biochemical sensor array, the processing paths, and the multiplexer and ADC for sampling. It is responsible for reading out the concentrations of lactate, glucose, K^+ , Na^+ , H^+ , Cl^- , and the temperature of human sweat.

When enough energy is harvested the biochemical sensing module and the backscatter communication module are activated. First of all the low-power FPGA is reconfigured from

non-volatile flash and starts working. Then the biochemical sensing module conducts a round of sensor reading over all the processing paths under the control of FPGA. The next step is using backscatter technology to transmit those sensor readings: the packet detection algorithm is executed to find ongoing BLE packets. Once a BLE packet is detected, the tag data modulation module starts sensor data transmission by toggling the RF-switch. After the modulation finishes sensor data transmission, the next round sensor reading and tag transmission start again. Such a procedure will repeat till stored power is insufficient.

III. BACKSCATTER COMMUNICATION

A. Carrier selection

For choosing a proper carrier device, our consideration focuses on the most widely used WiFi, Bluetooth, and LTE devices deployed in almost every smartphone and tablet. An investigation on the received signal strength indicator (RSSI) of WiFi, Bluetooth, LTE is conducted on the campus. The result is shown in Fig. 3(a). The ambient WiFi has the highest RSSI of around -40dBm in indoor environments, while in the same scenarios BLE and LTE are about -20dB lower. In other places, the situation will be similar.

Those signals are improper to act as the backscatter carrier. Backscatter requires a higher RSSI than ambient signals because backscatter has no such structures as amplifier to get high signal amplitude for detection. Still, after the reflection of the backscatter tag, the RSSI will drop by more than 30dB [19] and the reflected signal is too weak and the backscatter range is thus limited.

We also find that widely deployed tiny BLE devices such as wireless BLE headsets and smartwatches have RSSI as high as -23dBm (the “Body area BLE”) at the human wrist because of the close distance. The WiFi RSSI from smartphones at hand is even stronger. But considering WiFi’s higher unit cost and power consumption (\$7.19, 669mW) comparing to BLE (\$1.78, 27.3mW)¹ we think BLE is a better choice.

¹The prices and power consumptions of WiFi and BLE are based on commercial-off-the-shelf TI’s WiFi and BLE chipsets.

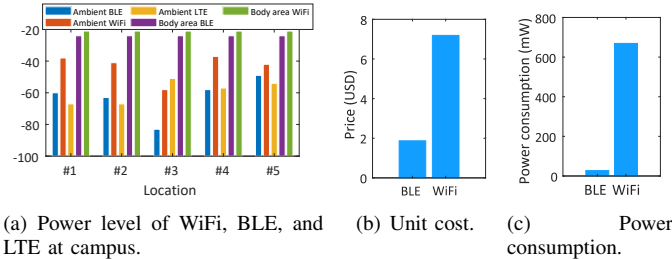


Fig. 3. RF front for BLE baseband envelope. In (a) location #1 is the Lab, location #2 is the dining hall, location #3 is the playground, location #4 is the classroom, and location #5 is the student dormitory. (b) and (c) are the comparisons of BLE with WiFi in unit cost and power consumption.

B. BLE packet identification

For the purpose of packet-detection, active BLE radios firstly down-convert received signal from the 2.4GHz Industrial Scientific Medical (ISM) frequency band to baseband, then conduct pulse shaping, carrier frequency offset correction, and cross-correlation with a pre-defined sequence. That processing flow will consume too much energy for our battery-free sweat monitoring system. We take the idea from the WISP and Multiscatter [20] [11] to directly use a rectifier to extract the baseband envelope which can be seen as the absolute value of the baseband signal.

The RF rectifier leverages the unidirectional conductivity of diodes so that in the positive cycle of received RF signal the capacitor can be charged quickly via the diodes. When the RF signal is negative the diodes are not conductive so the capacitor can only discharge slowly. In this way, the output waveform keeps only the baseband envelope. We can observe that the DC component is quite strong in the extracted BLE baseband. It takes up about 99% of total energy, and the AC component covers only about 1%. While for 802.11b WiFi and 802.11n WiFi envelopes, the DC components take about 77% and 47% energy, respectively. Such a significant difference is caused by different bandwidths and modulation schemes. A sliding window of size w is used to separate the DC and AC components in real time: $D(p) = \frac{\sum_{i=0}^{w-1} V_{base}(p-i)}{w}$, and $A(p) = V_{base}(p) - D(p)$ where the $V_{base}(p)$, $D(p)$, and $A(p)$ are the sampled envelope data, the DC and AC components, respectively. For reduction of computation complexity, we calculate the ratio of AC power and DC power in a simplified way as: $AC/DC = \frac{\sum_{p=1}^L |A(p)|}{\sum_{p=1}^L D(p)}$ where the L is the number of points used for BLE packet detection. The result is shown in Fig. 4(a). In about 98% cases it is below 0.06. For WiFi, it's above 0.4, which is much larger. And ZigBee has an AC/DC value over 0.08, slightly larger than that of BLE. That means BLE packets can be identified from other commercial packets in the 2.4GHz ISM band using AC/DC.

The interference such as WiFi and ZigBee packets can be filtered out from BLE using the AC/DC method, but to further confirm the existence of BLE packets, the cross-correlation of $A(p)$ and a pre-stored sequence $S(p)$ is also conducted. For reduction of computation complexity we use

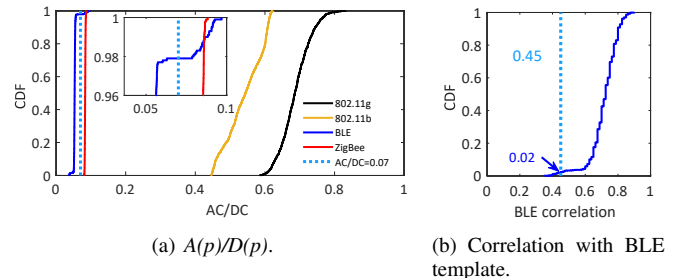


Fig. 4. BLE packet identification.

the sign of $A(p)$ and the sign of $S(p)$ in the calculation of cross-correlation: $R(i) = \frac{\sum_{p=1}^L sign(A(p-i))sign(S(p))}{\sqrt{\sum_{p=1}^L sign(A(p))}\sqrt{\sum_{p=1}^L sign(S(p))}} = \frac{\sum_{p=1}^L sign(A(p-i))sign(S(p))}{L}$. So that the calculation of cross-correlation can be simplified to 1-bit addition, which can be easily achieved by the low-power FPGA. The $R(i)$ result of 1000 packets (those packets are collected in the lab where RSSI ambient signals is below -40dBm) is shown in Fig. 4(b). For over 98% of packets, the cross-correlation is above 0.45. Our method is if AC/DC is lower than 0.07 and the cross-correlation result is above 0.45 the packet will be identified as a BLE packet. We use AC/DC and cross-correlation for BLE identification. For detecting BLE packets we have two methods. The first is using the cross-correlation and identify the current packet to BLE if the cross-correlation $R > Th_1$ where Th_1 is a threshold to filter out interference packets. The second method is combining cross-correlation and AC/DC , and only when $R > Th_2$, $AC/DC < Th_3$ will the packet be identified to a BLE packet, and the false detection can be controlled by setting Th_2 and Th_3 .

After BLE packet detection, the backscatter takes the “Codeword translation” introduced in FreeRider [21] for data transmission. In BLE packets, information is encoded in the frequency. Let f_0 be the frequency for bit ‘0’ and f_1 for bit ‘1’. If sensor data is bit ‘0’, the backscatter introduces an additional frequency shift so that there will be a transition between f_0 and f_1 in the excitation packet, causing a difference in the information bit. Instead, if tag data is bit ‘0’ the codeword translation is not conducted and the contained information is not changed.

IV. POWER MANAGEMENT

Harvesting energy from ambient energy sources such as light, vibration, thermal, wind, radio-frequency signal, and other potential sources widespread in the environment is a good choice for replacing batteries. We use a solar panel, a thermoelectric generator (TEG), and a rectifier circuit composed of diodes and capacitors for the harvesting of light energy, thermal energy, and RF energy, respectively.

A. Comprehensive use of three energy sources

The solar panel, the TEG, and the rectifier have different electrical characteristics in nature. Our testing shows that with $10^\circ C$ TEG has a resistor as low as 6.12Ω , which is much

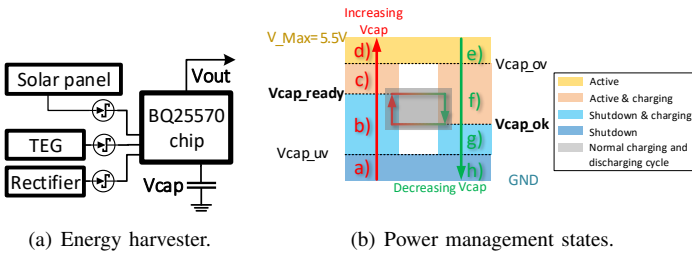


Fig. 5. Power harvesting and managing.

lower than that of the solar panel ($119K\Omega$) with 500Lux light, and the rectifier with 0dBm RF signal ($1.09M\Omega$). Still, the generated DC voltage at $10^\circ C$ by the TEG is only about 0.31V, which is much lower than that of the other two sources (both the solar panel and the rectifier has an output voltage above 1.5V), too.

If those harvesting devices are connected to the power management chip (the TI BQ25570 harvesting management chip in Apollo system) directly, the TEG will act as a load and waste a large portion of energy. When the solar panel is the only available energy source, the TEG, the rectifier, and the BQ25570 power management chip are connected in parallel and act as the load. As the TEG has a resistor as low as 6.12Ω which is significantly smaller than the rectifier and the BQ25570 chip, it will dissipate a majority of total energy and cause power harvesting failure.

So those harvesting devices should be isolated in some way. For this purpose, complex devices that need control signals such as multiplexers shouldn't be used because the control signals come after energy supply. In our design, the unidirectional conductivity of diodes is utilized. As Fig. 5(a) shows every harvesting device is connected to the BQ25570 chip via a low-dropout Schottky diode. Then the equivalent resistors of the rectifier and the TEG are both quite high so that most of the harvested energy is conveyed to the BQ25570 chip for harvesting.

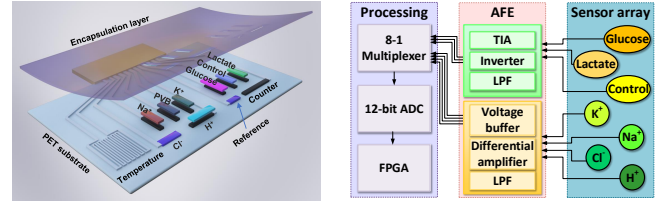
B. Charging and discharging

The system carries out BLE packet detection, sweat analyzing, and backscatter transmission, leading to a power consumption of about 20mW. The TI harvesting management chip BQ25570 is employed to ensure the normal operation of the system. Our system either keeps active to operate normally when stored energy is adequate, or shuts down to charge the storage capacitor at full speed.

According the voltage V_{cap} and its rising or dropping edge, there are four different states:

Shutdown $V_{cap} < V_{cap_uv}$ in both rising and dropping edges: The system is shut down and the storage capacitor is charged quite slowly because the functionality of BQ25570 chip is influenced by the low V_{cap} . This state exists when the storage capacitor is charged from empty, or all energy sources become unavailable and V_{cap} drops below V_{cap_uv} .

Shutdown&charging ($V_{cap_uv} < V_{cap} < V_{cap_ready}$ (in rising



(a) Structure illustration of the six-channel electrode array to detect glucose, lactate, Na^+ , K^+ , H^+ , and Cl^- .
(b) Biochemical signal conditioning channel electrode array to detect glucose, lactate, Na^+ , K^+ , H^+ , and Cl^- .

Fig. 6. Biochemical sensing structure.

edge), or $V_{cap_uv} < V_{cap} < V_{cap_ok}$ (in dropping edge)): the system is in shutdown state and the storage capacitor is charged normally using harvested energy. If there is no available energy source V_{cap} will further drop (procedure g)), otherwise V_{cap} increases (procedure b)).

Active&charging ($V_{cap_ready} < V_{cap} < V_{ov}$ (in rising edge), or $V_{cap_ok} < V_{cap} < V_{cap_ready}$ (in dropping edge)): the system is in active state, and the sweat monitoring is conducted. The storage capacitor is charged normally but in most cases V_{cap} will drop quickly because of system consumption (procedure f)). But when energy sources are too strong and harvested energy is more than system consumption V_{cap} will further rise (procedure c)).

Active $V_{cap} > V_{cap_ov}$ in both rising and dropping edges: the system is active but the charging is stopped to protect the storage capacitor.

The normal situation is that V_{cap} cyclicly stays in procedure b) (charging) and procedure f) (discharging). And the useful energy in a charging and discharging cycle is: $E_c = \frac{1}{2}C_{store}V_{cap_ready}^2 - \frac{1}{2}C_{store}V_{cap_ok}^2$. Every time the power supply is recovered the system uses the energy of E_c to read and transmit sensor data.

V. ENERGY-EFFICIENT SWEAT SENSING

This part explains how to sense human sweat in an energy-efficient way. For the purpose of sensing sweat, a customized biochemical sensor array and signal processing circuits are integrated into our Apollo system. For glucose and lactate, the working electrodes are modified by glucose oxidase and lactate oxidase respectively, and for Na^+ , K^+ , H^+ , and Cl^- the corresponding ion-selective electrodes are used as shown in Fig. 6(a). Then current signal (glucose, lactate) or voltage signal (Na^+ , K^+ , H^+ , and Cl^-) will be generated by the corresponding chemical reactions, and the signal amplitudes are determined by the concentrations. The structure of signal conditioning analog front end (AFE) to make the converted electric signal acceptable by the processing circuit, and the signal processing circuit to sample and process the conditioned electric information are shown in Fig. 6(b). And to filter out interference from other sweat compositions, the differential-measurement method is employed. We set a reference electrode without glucose oxidase or lactate oxidase, and the real

electric signal is the difference between the working electrode and the reference electrode.

VI. IMPLEMENTATION

The wearable biochemical system is built on a 2-layer 145mm×45mm wristband-shaped flexible printed circuit board. Our biochemical sensor electrodes are customized, and all other components are commercial-off-the-shelf components.

A. Backscatter communication

In the system, a Microsemi IGLOO nano AGLN250 FPGA works as the controller for the packet detection algorithm and the toggling control of RF-switch. The RF switch ADG902 is used to reflect the RF signal and realize data transmission. To get a fine-grained baseband envelope we use a high-bandwidth rectifier composed of the Schottky diodes HSMS-286C, capacitors, and resistors. The baseband envelope is sampled by a low-power ADC LTC2366. To provide WiFi (802.11b/n), BLE, and ZigBee packets for testing and evaluation, we use laptops with the AR938X wireless network adapter, the TI CC2540 BLE module, and the TI CC2530 ZigBee module, respectively.

B. Energy harvesting

For harvesting light energy, heat energy, and RF energy, a solar cell MP3-37 (size: 114mm×37mm), 6 thermoelectric generators TG12-8-01LS connected in series (size: 40mm×40mm), and a 5-stage voltage doubler circuit composed of capacitors and the HSMS-286C Schottky diodes are used, respectively. And the TI energy harvesting chip BQ25570 which supplies 3.3V DC power is used in our system to manage charging and discharging. Considering the serious current leakage which will lead to power dissipation in a large capacitor, and the limited storage capacity of a small capacitor, we use a 1000uF capacitor to store harvested energy.

C. Sweat sensing

We use the operational amplifiers LT1462, capacitors, and resistors to build the signal processing circuit paths. To satisfy the needed ±5V power rails by the LT1462, we use the booster converter TPS61220 to convert the 3.3V system supply to 5V. And the charge pump voltage inverter TPS60400 is used for -5V. As mentioned before the processed signals by processing paths for glucose, lactate, K^+ , Na^+ , H^+ , and Cl^- need to be sampled by ADC. The multiplexer ADG758 is used to connect one of those paths to the low-power ADC AD7466 for sensor reading.

D. Power consumption

In our prototype, the total consumption is about 23.88mW, including 18.08mW of backscatter part (FPGA: 10.11mW, ADC: 7.2mW, Oscillator: 0.59mW, and RF switch: 0.18mW) and 5.8mW of the biochemical signal processing circuits.

To illustrate the power reduction by using backscatter technology, we compare the energy to transmit 1-bit data by

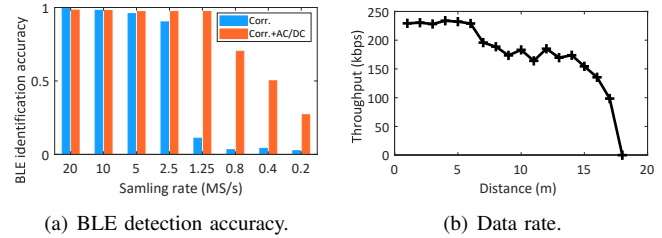


Fig. 7. Backscatter communication capability.

backscatter and the commercial Bluetooth devices. For fairness, the method introduced in BLE-backscatter [22] is taken. In commercial BLE devices including Nordic nRF51822 and TI CC2650, only the datasheet-supplied energy consumption of the frequency synthesizer and transmission is counted. In our system the RF switch consumes 0.18mW to transmit data at about 250kbps, corresponding to 720pJ/bit. For Nordic nRF51822 it's 18.9nJ/bit, and for TI CC2650 it's 18.3nJ/bit. We can see that backscatter realizes a 26× power reduction.

And the power consumption of biochemical sensors and processing circuits is 5.80mW, which is much lower compared to the electrochemical workstation. For example, the electrochemical workstation model 700E series instrument of CH instruments, Inc. consumes tens of Watts.

VII. EVALUATION

A. Backscatter communication

1) Packet detection: Now we investigate backscatter communication capability. We first evaluate the BLE packet detection rate over the sampling rate. The commodity TI CC2540 BLE module with RSSI no more than 4dBm is used as the carrier source, and it is placed about 0.2m from the backscatter to simulate the usage scenario with human. We compare the BLE detection performance with correlation only ($R > Th_1$), or combining correlation and AD/DC ($R > Th_2, AC/DC, Th_2$) when the false detection rate of other packets including WiFi and ZigBee are kept below 5%.

The experiment result is shown in Fig. 7(a). Both methods achieve detection rates over 90% when the sampling rate is above 2.5MS/s. But using cross-correlation only the detection rate is below 10% at 1.25MS/s. While combining AC/DC and cross-correlation the detection rate is still above 95% at 1.25MS/s, and above 70% at 0.8MS/s, significantly improving detection performance.

2) Transmission performance: The throughput over distance is evaluated in a hallway of a teaching building. The transmission power is boosted to about 20dBm using an amplifier. The backscatter tag is provided with external power and placed about 0.2m from the transmitter. Four carrier symbols of 1Mbps BLE packets are used to transmit 1-bit backscatter data. Fig. 7(b) shows the throughput of our backscatter system with increasing range. The maximum operational distance is 17m. The throughput drops with an increase in distance. Within the distance of 6m, the throughput is above 200Kbps, and within 15m the throughput is still above 150Kbps. Such

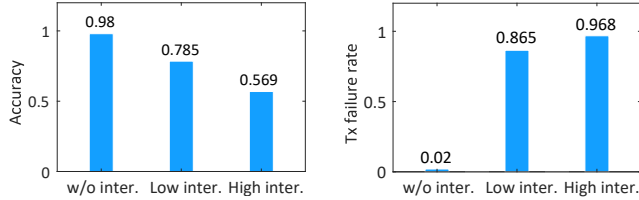


Fig. 8. The influence of interference on backscatter transmission.

TABLE I
TIME TO CHARGE THE SUPER CAPACITOR FROM V_{cap_ok} TO V_{cap_ready}

Available energy source	Only available via no diodes	All connected via no diodes	All connected via diodes
500Lux light	21.6s	—	26.8s
10°C TEG	3.39s	3.48s	5.80s
6dBm RF	2.64s	—	2.84s

communication performance is enough for our sweat monitoring system.

3) *Detection with interference and BLE detection power efficiency:* We set a WiFi radio (a PC with Qualcomm Atheros AR938X NIC) to generate 802.11n packets with payload of 500 bytes at rates of 0pkts/s (w/o interference), 300pkts/s (low interference), and 1000pkts/s (high interference) as interference source. The corresponding BLE detection rates with sampling rate of 1.25Msps are 0.98, 0.785, and 0.569, as shown in Fig. 8(a). The reduction in detection rate is caused by the collision with WiFi packets.

The overall power consumption is about 23.88mW. If we don't carry out BLE packet detection and simplify the system to monitoring the RSSI using a comparator to find carrier packets, the consumption can be reduced to about 17mW. But we should notice that with WiFi interference which has a much higher packet rate comparing to BLE (~30pkts/s advertising packet rate), the RSSI method is very likely to fail, as Fig. 8(b) shows. When the failure rate is high, frequently retransmission is needed, causing more power dissipation. For example, the failure rate is about 0.865 with low interference, meaning that a backscatter packet needs 7.4 times repeated transmission on average. With BLE packet detection, such retransmission can be avoided, and more power can be saved.

B. Power harvesting

As mentioned we use Schottky diodes to avoid interference between multiple energy converters. To show the effectiveness we test the time to charge the storage capacitor from V_{cap_ok} (2.60V) to V_{cap_ready} (4.10V) using different energy sources, the results are shown in Table. I. Without diodes, the light energy and RF energy would not be harvested and stored because of the dissipation of TEG. After diodes are attached energy can be harvested and stored normally, but there will be a charging time increase of about 24%, 71%, and 7.6% light energy, heat energy, and RF energy, respectively. Such an

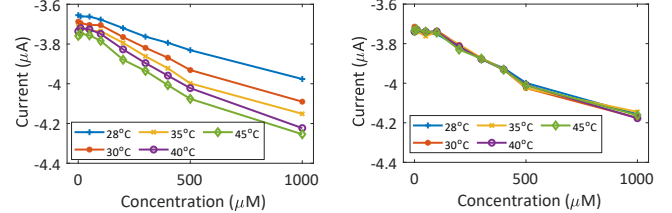


Fig. 9. System level real-time temperature compensation for the glucose.

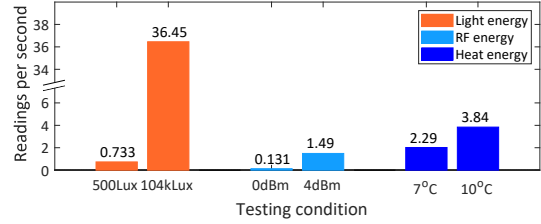


Fig. 10. Reading rate with different energy sources.

increase is caused by the forward voltage of Schottky diodes, but we think it's still acceptable comparing to wider energy sources.

C. Sweat sensing and analyzing

The temperature will significantly influence sweat sensing. The example of glucose is shown in Fig. 9(a). The response current rises when glucose concentration or temperature increases. Thus the temperature causes ambiguity in glucose measuring results. For example, when the tested current is $3.98\mu A$ the glucose may be about $1000\mu M$ (at $28^\circ C$), $650\mu M$ (at $30^\circ C$), or $370\mu M$ (at $45^\circ C$)... So we compensate for the influence of temperature using a 4th order polynomial. After compensation, the current-concentration curves under different temperatures converge and the fluctuation caused by temperature is negligible as shown in Fig. 9(b). The error of inferred glucose concentration from reverse current is below 5% in the temperature range of $28^\circ C \sim 40^\circ C$. Such performance is comparable to 10% error using laser [23]. In our design, the sensor temperature used for compensation is measured using a built-in temperature sensor in the sensor array.

D. Real-time sensor reading and data transmitting

We test the system performance with harvested energy. Other experiment setup is similar to that in Section. VII-A. As shown in Fig. 10, when harvesting from office light (500Lux) or sunlight (104000 Lux), the effective tag packet rates are 0.733 pkts/s and 36.45pkts/s, respectively (light of about 10700 Lux is enough to supply energy for the system to work continuously and realize similar performance). With RF energy or human heat, the tag packet rates reach 1.49pkts/s and 3.84pkts/s, respectively. We can see that harvesting thermal energy is efficient and stable. But the rigid TEG needs to be

stuck close to the human body, influencing normal activity. Harvesting light and RF energy wouldn't influence human activity, but they are not always accessible. So combining them helps extend the usage scenario.

VIII. RELATED WORK

Backscatter communication is attractive for its connectivity with the lowest power consumption. Many works including Passive WiFi [24], Interscatter [25], HitchHike [26], FreeRider [21], X-Tadem [27] make great progress towards commercial-devices compatibility of backscatter. The key strengths of backscatter are its low power consumption, simple structure, and small size, which help to satisfy the requirements of wearable, self-powered, and long-range.

For satisfying self-powered requirements, we still need to consider the harvestable energy source. WISP [28] [29] follows the idea of the radio-frequency identification (RFID) to utilize the radio-frequency power which comes from the high-cost RFID reader as the energy source. PLoRa [30] and Tunnelscatter [31] focus on light power harvesting. Whole the RF-powered system needs an expensive reader as the source of RF energy, and the light-powered system has an unstable performance because light condition changes with the environment. So our system harvests energy from not only RF energy and light, but also from the heat of the human body which is a relatively stable source.

IX. CONCLUSION

This work introduces Apollo biosensor system. It's capable of harvesting multiple ambient energies, monitoring human sweat, and realizing sensor reading transmission range of about 17m. And to our knowledge we are the first to embed backscatter communication and biochemical sensing technology in the wearable sensor system.

ACKNOWLEDGMENT

This work was supported by NSFC Grant No. 61932017 and 61971390, and Hefei Healthcare Grant No. J2020Y03. The authors would like to thank the Information Science Laboratory Center of USTC for the hardware/software services.

REFERENCES

- [1] A. Nemirovski, D. C. Christodouleas, J. W. Hennek, A. A. Kumar, E. J. Maxwell, M. T. Fernández-Abedul, and G. M. Whitesides, "Universal mobile electrochemical detector designed for use in resource-limited applications," *Proceedings of the National Academy of Sciences*, vol. 111, no. 33, pp. 11 984–11 989, 2014.
- [2] W. Gao, S. Emaminejad, H. Y. Y. Nyein, S. Challa, K. Chen, A. Peck, H. M. Fahad, H. Ota, H. Shiraki, D. Kiriyama *et al.*, "Fully integrated wearable sensor arrays for multiplexed *in situ* perspiration analysis," *Nature*, vol. 529, no. 7587, pp. 509–514, 2016.
- [3] Y. Yang, Y. Song, X. Bo, J. Min, O. S. Pak, L. Zhu, M. Wang, J. Tu, A. Kogan, H. Zhang *et al.*, "A laser-engraved wearable sensor for sensitive detection of uric acid and tyrosine in sweat," *Nature Biotechnology*, vol. 38, no. 2, pp. 217–224, 2020.
- [4] G. Xu, C. Cheng, Z. Liu, W. Yuan, X. Wu, Y. Lu, S. S. Low, J. Liu, L. Zhu, D. Ji *et al.*, "Battery-free and wireless epidermal electrochemical system with all-printed stretchable electrode array for multiplexed *in situ* sweat analysis," *Advanced Materials Technologies*, vol. 4, no. 7, p. 1800658, 2019.
- [5] H. Liu, W. Gong, X. Miao, K. Liu, and W. He, "Towards adaptive continuous scanning in large-scale rfid systems," in *Proc. of IEEE INFOCOM*, 2014.
- [6] H. Liu, W. Gong, L. Chen, W. He, K. Liu, and Y. Liu, "Generic composite counting in rfid systems," in *Proc. of IEEE ICDCS*, 2014.
- [7] W. Gong, J. Liu, and Z. Yang, "Fast and reliable unknown tag detection in large-scale rfid systems," in *Proc. of ACM MobiHoc*, 2016.
- [8] K. Liu, Q. Ma, W. Gong, X. Miao, and Y. Liu, "Self-diagnosis for detecting system failures in large-scale wireless sensor networks," *IEEE Transactions on Wireless Communications*, vol. 13, no. 10, pp. 5535–5545, 2014.
- [9] W. Gong, I. Stojmenovic, A. Nayak, K. Liu, and H. Liu, "Fast and scalable counterfeits estimation for large-scale rfid systems," *IEEE/ACM transactions on networking*, vol. 24, no. 2, pp. 1052–1064, 2015.
- [10] W. Gong, J. Liu, and Z. Yang, "Efficient unknown tag detection in large-scale rfid systems with unreliable channels," *IEEE/ACM Transactions on Networking*, vol. 25, no. 4, pp. 2528–2539, 2017.
- [11] W. Gong, L. Yuan, Q. Wang, and J. Zhao, "Multiprotocol backscatter for personal iot sensors," in *Proc. of ACM CoNEXT*, 2020.
- [12] J. Zhao, W. Gong, and J. Liu, "Spatial stream backscatter using commodity wifi," in *Proc. of ACM Mobicys*, 2018.
- [13] W. Gong, H. Liu, J. Liu, X. Fan, K. Liu, Q. Ma, and X. Ji, "Channel-aware rate adaptation for backscatter networks," *IEEE/ACM Transactions on Networking*, vol. 26, no. 2, pp. 751–764, 2018.
- [14] J. Zhao, W. Gong, and J. Liu, "X-tandem: Towards multi-hop backscatter communication with commodity wifi," in *Proc. of ACM Mobicom*, 2018.
- [15] W. Gong, S. Chen, J. Liu, and Z. Wang, "Mobirate: Mobility-aware rate adaptation using phy information for backscatter networks," in *IEEE INFOCOM*, 2018.
- [16] W. Gong, S. Chen, and J. Liu, "Towards higher throughput rate adaptation for backscatter networks," in *Proc. of IEEE ICNP*, 2017.
- [17] J. Zhao, W. Gong, and J. Liu, "Towards scalable backscatter sensor mesh with decodable relay and distributed excitation," *Signal*, vol. 90, p. 80, 2020.
- [18] Q. Wang, J. Yu, C. Xiong, J. Zhao, S. Chen, R. Zhang, and W. Gong, "Efficient backscatter with ambient wifi for live streaming," in *Proc. of IEEE Globecom*, 2020.
- [19] D. M. Dobkin, *The rf in RFID: uhf RFID in practice*. Newnes, 2012.
- [20] M. Philipose, J. R. Smith, B. Jiang, A. Mamishev, S. Roy, and K. Sundara-Rajan, "Battery-free wireless identification and sensing," *IEEE Pervasive computing*, vol. 4, no. 1, pp. 37–45, 2005.
- [21] P. Zhang, C. Josephson, D. Bharadia, and S. Katti, "Freerider: Backscatter communication using commodity radios," in *Proc. ACM CoNEXT*, 2017.
- [22] J. F. Ensworth and M. S. Reynolds, "Ble-backscatter: Ultralow-power iot nodes compatible with bluetooth 4.0 low energy (ble) smartphones and tablets," *IEEE Transactions on Microwave Theory and Techniques*, vol. 65, no. 9, pp. 3360–3368, 2017.
- [23] T. Li, D. Bai, T. Prioleau, N. Bui, T. Vu, and X. Zhou, "Noninvasive glucose monitoring using polarized light," in *Proc. of ACM SenSys*, 2020.
- [24] B. Kellogg, V. Talla, S. Gollakota, and J. R. Smith, "Passive wi-fi: Bringing low power to wi-fi transmissions," in *Proc. ACM USENIX NSDI*, 2016.
- [25] V. Iyer, V. Talla, B. Kellogg, S. Gollakota, and J. Smith, "Inter-technology backscatter: Towards internet connectivity for implanted devices," in *Proc. ACM SIGCOMM*, 2016.
- [26] P. Zhang, D. Bharadia, K. Joshi, and S. Katti, "Hitchhike: Practical backscatter using commodity wifi," in *Proc. ACM SenSys*, 2016.
- [27] J. Zhao, W. Gong, and J. Liu, "X-tandem: Towards multi-hop backscatter communication with commodity wifi," in *Proc. ACM MobiCom*, 2018.
- [28] M. Philipose, J. R. Smith, B. Jiang, A. Mamishev, S. Roy, and K. Sundara-Rajan, "Battery-free wireless identification and sensing," *IEEE Pervasive computing*, vol. 4, no. 1, pp. 37–45, 2005.
- [29] A. P. Sample, D. J. Yeager, P. S. Powledge, A. V. Mamishev, and J. R. Smith, "Design of an rfid-based battery-free programmable sensing platform," *IEEE transactions on instrumentation and measurement*, vol. 57, no. 11, pp. 2608–2615, 2008.
- [30] Y. Peng, L. Shangguan, Y. Hu, Y. Qian, X. Lin, X. Chen, D. Fang, and K. Jamieson, "Plora: A passive long-range data network from ambient lora transmissions," in *Proc. of ACM SIGCOMM*, 2018.
- [31] A. Varshney, A. Soleiman, and T. Voigt, "Tunnelscatter: Low power communication for sensor tags using tunnel diodes," in *Proc. of ACM Mobicom*, 2019.